

University of California
Ernest O. Lawrence
Radiation Laboratory

CHARGE DISTRIBUTIONS OF PRODUCTS
OF REACTIONS BETWEEN COMPLEX NUCLEI

TWO-WEEK LOAN COPY

*This is a Library Circulating Copy
which may be borrowed for two weeks.
For a personal retention copy, call
Tech. Info. Division, Ext. 5545*

Berkeley, California

DISCLAIMER

This document was prepared as an account of work sponsored by the United States Government. While this document is believed to contain correct information, neither the United States Government nor any agency thereof, nor the Regents of the University of California, nor any of their employees, makes any warranty, express or implied, or assumes any legal responsibility for the accuracy, completeness, or usefulness of any information, apparatus, product, or process disclosed, or represents that its use would not infringe privately owned rights. Reference herein to any specific commercial product, process, or service by its trade name, trademark, manufacturer, or otherwise, does not necessarily constitute or imply its endorsement, recommendation, or favoring by the United States Government or any agency thereof, or the Regents of the University of California. The views and opinions of authors expressed herein do not necessarily state or reflect those of the United States Government or any agency thereof or the Regents of the University of California.

For meeting and proceedings of 3rd Conference
on Interactions Between Complex Nuclei -
Asilomar, April 15-17, 1963

UNIVERSITY OF CALIFORNIA

Lawrence Radiation Laboratory
Berkeley, California

Contract No. W-7405-eng-48

CHARGE DISTRIBUTIONS OF PRODUCTS OF REACTIONS

BETWEEN COMPLEX NUCLEI

Naftali H. Steiger

April 5, 1963

CHARGE DISTRIBUTIONS OF PRODUCTS OF
REACTIONS BETWEEN COMPLEX NUCLEI²⁺

Naftali H. Steiger†

Lawrence Radiation Laboratory
University of California
Berkeley, California

April 5, 1965

In recent years the detailed study of properties of recoiling nuclei has been an important source of information on nuclear reaction mechanism.¹ This method has been especially useful for the investigation of reaction mechanisms between complex nuclei.²⁻⁴ In this case heavy reaction products of considerable energy may be obtained.

Interpretation of these studies would be improved by knowledge of the distribution of effective charges of the heavy particles generated in the nuclear reaction investigated.

We present here the results of an experimental study of effective charge-state distributions of products of heavy-ion-induced nuclear reactions, in the rare earth region. We give results of a detailed study of equilibrium charge distributions, as well as some first results on "instantaneous" charges, obtained before equilibrium is reached.

When heavy particles pass through matter they can lose or capture electrons in collisions with the stationary atoms of the medium traversed. This very complicated process results in the establishment of an equilibrium distribution of charges. From such a distribution the characteristic mean charge may be obtained, which will relate to an element of the path of the penetrating particle; this path is long enough to include a large number of charge exchange collisions, but too short for any appreciable slowing down of the particle.

In general, and qualitatively, we know that the equilibrium mean charge $\langle z \rangle$ of a particle when passing through matter is given by

$$z = f(Z_1 A_1 \vee Z_2 A_2, \text{state of condensation of medium}). \quad (1)$$

There is not at present any rigorous theory about the charge distribution of heavy particles as a function of the various factors shown. Only in the case of hydrogen atoms moving in a medium of atomic H, a quantum mechanical approach has been successfully used.⁵ Other methods used are approximate in character; they are mainly based on statistical considerations and are not in very satisfactory agreement with the experiments.⁶⁻¹¹ Empirical factors have therefore been introduced in order to allow for these discrepancies.

The existing experimental data are mostly for Z_1 up to about 18 (Argon), because until now the possibilities of accelerating "very heavy" ions, ($Z_1 > 18$) have been limited. Measurements have been performed on fission fragments, but because of their continuous spread in Z_1 , they can be related only roughly to $Z = 38$ (Sr) and $Z = 54$ (Xe) as the most representative ones.^{12,13}

Spallation products resulting from heavy-ion-induced nuclear reactions can be produced in a wide energy interval, from a few MeV up to a few tens of MeV. This offers therefore an almost unique possibility for the study of charge equilibrium of heavy particles possessing even higher Z_1 than the fission fragments. The data presented here are for a study of equilibrium charge distributions of heavy particles of nuclear charge $Z_1 = 66 \pm 1$ (Tb, Dy, Ho) in a velocity region from about 2.5×10^8 cm/sec to about 6×10^8 cm/sec; in atomic units this corresponds to about 1 to almost 3 times the velocity of an electron in the hydrogen atom.

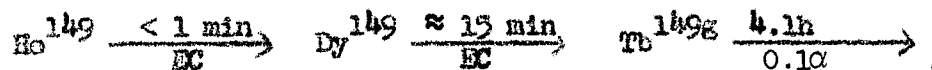
EXPERIMENTAL PROCEDURE

In choosing the nuclear reactions to be utilized the intention was to find a number of reactions which ideally all lead to the same primary spallation product, and which should result in as wide a velocity range as possible.

A number of reactions, all of the type (HI, xn) , were therefore chosen, most of them leading to ${}^{66}\text{Dy}^{149}$ as the primary spallation product. For covering a certain velocity range of the resulting heavy particles, reactions leading to ${}^{65}\text{Tb}^{149g}$ as well as reactions leading to ${}^{67}\text{Ho}^{149}$ were also chosen. The study had to be limited to reactions for which evidence for compound-nucleus mechanism has been presented,^{2,3} because only in this case are we able to calculate the mean velocity of the spallation products.

A schematic representation of the experimental setup is shown in Fig. 1. The heavy-ion beam, deflected by a bending magnet through 30 deg, enters the experimental chamber through a small oval collimator and penetrates an appropriate number of degrading foils. The bombarding energy was varied, usually around the peak of the excitation function of a particular reaction, so long as the reaction cross section still allowed reasonable reaction yields. In this way the velocity of the resulting products from a certain reaction was varied to some extent. The somewhat scattered heavy ions emerging from the last degrading foil hit the target after passing a narrow slit collimator and penetrating the backing material. The resulting reaction products together with the heavy-ion beam pass an additional slit collimator and enter the gap of a permanent magnet of 3150 gauss field strength. The charged spallation products, as well as the beam ions, are horizontally deflected according to their momenta and effective charge states. The spallation products are finally collected on a thin Al catcher foil. The Faraday cup behind the catcher foil serves to monitor the heavy-ion beam throughout the experiment.

As all three types of spallation products obtained in the various cases are genetically related and decay to Tb^{149g} ,



the same detecting method was used for all the reactions, namely the counting of the α tracks of the decaying Tb^{149g} on a nuclear track emulsion.

The horizontal distribution of the collected spallation products was thus recorded by taking an autoradiograph of the catcher foil, and the plate was finally scanned for α -track density as a function of the horizontal distance from the beam axis. On the place on the plate corresponding to where the heavy-ion beam was hitting the catcher foil, a line was obtained indicating β activity induced in the catcher foil and its plastic cover. Furthermore, long-range α tracks, which could be clearly distinguished from the short-range rare earth α tracks, were found in this place. These tracks were attributed to α activity induced in heavy-element impurities existing in the catcher foil material. (See induced α -activity peaks on Fig. 2.) The position of the beam axis on the catcher foil, which corresponds to the zero-deflection position of the particles, was obtained for each run by a short calibration run, without target and with no magnetic field applied. As under the experimental conditions applied, the heavy-ion beam was practically completely stripped,¹⁴ the distance between the zero-deflection position and the position of the deflected beam was used for the calibration of the charge-state scale. All the experiments were performed at a pressure of about 10^{-4} mm.

EXPERIMENTAL ANALYSIS

On the basis of the fundamental equation for magnetic deflection of charged particles and from pure geometrical considerations of the experimental setup, we find that the horizontal deflection x on the catcher foil, with respect to the beam axis of a particle of mass m , velocity v and effective charge state z , is given by

$$x = \frac{A_1 c v}{Hez} \left[1 - \cos\left(\arcsin \frac{lHez}{A_1 c v}\right) \right] + Ll \frac{Hez}{A_1 c v} \frac{1}{\cos\left(\arcsin \frac{lHez}{A_1 c v}\right)} \quad (2)$$

where H is the magnetic field strength, c the velocity of light, e the elementary charge, l the length of the magnetic field, and L the distance between the end of the magnetic field and the catcher foil.

The various charge states of the deflected spallation products were thus identified by use of Eq. (2), introducing for A_1 the mass of the final nuclear reaction product, and for v the mean velocity $\langle v \rangle$ of these products (see Eq. (3).)

In order to calculate the velocity of the spallation products we have to consider the mechanism of the reactions by which they are produced. The nuclear reactions studied and the bombarding conditions applied are summarized in the first two columns of Table I. Experimental investigations of the recoil properties of the final products of reactions of this type have provided a test for the validity of the statistical assumption and were found to favor a "compound nucleus" reaction mechanism.^{2,3,15} The excitation energies obtained in these reactions vary between about 35 and 125 MeV. At such high energies of excitation a very large number of overlapping levels will exist. If we assume that in the outgoing channels the random-phase approximation still applies, the angular distribution of the evaporated neutrons should be symmetric about $\pi/2$ in the center-of-mass system. Let us therefore assume that an incident beam particle of lab energy E_p is absorbed to form an excited state of a compound nucleus. As in any model for a nuclear reaction, linear

where Q is the mass difference between reactants and final products, and T_γ is the average total energy of the system emitted as photons. The recoil velocity due to the photon emission can be neglected.

The T_n values used here are based on Simonoff and Alexander's measurements¹⁵ of angular distributions of spallation products which result from reactions similar to those we have studied. These T_n values were obtained by them with the simplified assumption of isotropic neutron emission.

As is apparent from the experimental setup, a very highly collimated beam of reaction particles has been used in these experiments. Therefore, when trying to estimate the velocity spread, we may take into consideration only the velocity contributions of evaporation chains whose vector sums result in the forward and backward directions along the beam axis. Because of symmetric neutron evaporation, $\langle V \rangle$ will be zero. We then get, for the variance of the velocity relative to the square of the mean velocity,

$$\frac{\langle V^2 \rangle}{\langle v \rangle^2} = \frac{\left[\frac{E_b A_n^2}{A_b + A_T} \right] + Q + T_\gamma (A_b + A_T)^2}{E_b A_b (A_b + A_T - \frac{x+1}{2} m_n)^2} \quad (6)$$

This gives us an estimate of the velocity spread caused by neutron evaporation.

The velocity spread caused by target thickness was estimated from interpolation of experimental range-energy determinations of products of similar reactions in Al and Au.² For the "equilibrium experiments" the target thickness was usually of the order of 100 $\mu\text{g}/\text{cm}^2$, which allowed reasonable reaction yields. In the case of "nonequilibrium" experiments thinner targets, down to about 9 $\mu\text{g}/\text{cm}^2$, have been used. The velocity spread caused by stopping effects in the degrader could be neglected.

The geometrical spread was determined experimentally for each case. In Fig. 2 a typical experimental scanning curve is shown representing α -track density on the nuclear emulsion plate versus deflection distance on the plate. This distance is

equivalent to the horizontal deflection x of the charged reaction products obtained on the catcher foil. Two induced- α -activity peaks can be seen. The induced- α -activity peak obtained at the zero deflection position does not interfere with the main curve. However, the induced α activity produced by the deflected beam is superimposed on the experimental charge-distribution curve. These induced- α -activity curves were found by performing bombardments under conditions similar to those in a regular run, but using instead of the target an equivalent foil of its backing material only. In this way the experimental scanning curves obtained were corrected for the beam-induced α activity. The resultant curve was further corrected for velocity spread caused by neutron evaporation according to Eq. (6), for velocity spread caused by target thickness, and for geometrical spread. Finally the corrected curve was converted into a histogram for integer z values, representing the actual charge distribution for a certain velocity $\langle v \rangle$. In Fig. 3 an example of such a histogram is shown. This figure represents the equilibrium charge distribution of an Ho^{149} particle moving with a mean velocity of $\langle v \rangle = 4.5 \times 10^8$ cm/sec. The figure shows the relative probabilities of the different charge states obtained, ϕ_z (%), as a function of the ionic charge z .

momentum is conserved, the momentum of the incident beam particle is equal to the momentum of the compound nucleus. We then get, for the velocity of the compound nucleus,

$$v_{CN}^2 = \frac{2 A_b E_b}{(A_b + A_T)^2} \quad (3)$$

which is identical with the velocity of the center of mass. A_b and A_T denote the masses of bombarding particle and target atom respectively. As the compound nucleus decays, the velocities of the resulting spallation products are affected by this decay. However, when we recall the assumption of symmetric angular distribution of the evaporated neutrons, we get the result that the mean velocity (v) of the final products is equal to v_{CN} and therefore is given by Eq. (3).

In order to estimate the velocity spread caused by nucleon evaporation, let us consider somewhat further the decay of the compound nucleus.

Let \underline{V} denote the c.m. velocity given to the spallation products as a result of evaporation of all the neutrons. Let us for further simplification assume that the neutrons are emitted in random directions in the center-of-mass system. We can then find an expression for the mean square value of \underline{V} for this random walk. We get for the momentum of a recoiling mean mass of the evaporation chain,

$$\left[A_b + A_T - \frac{x+1}{2} m_n \right]^2 \langle V^2 \rangle = 2 T_n m_n \quad (4)$$

where $(A_b + A_T - \frac{x+1}{2} m_n)$ represents the "mean mass" of the heavy product during an evaporation process of x neutrons; T_n is the average total energy removed by the evaporated neutrons, and m_n is the mass of the neutron. T_n is given by,

$$T_n = E_b \frac{A_T}{A_b + A_T} + Q - T_\gamma \quad (5)$$

RESULTS AND DISCUSSION

A. Equilibrium Charge Distributions

In Table I are given a summary of the nuclear reactions studied, the bombarding conditions, and some of the obtained results.

In Table II are shown the relative probabilities for the charge states obtained, ϕ_z (%), as a function of the various particle velocities. Each vertical column corresponds to a certain type of nuclear reaction under certain bombardment conditions as shown in Table I. The probabilities given are the mean results of a number of repeated experiments.

In Fig. 4 we see some of these probabilities plotted as a function of velocity; smooth curves were obtained. The curves given are for the ionic charges 5, 10, 15, 20, and 25.

A rigorous theoretical treatment of the collisions between highly charged ions and atoms is extremely complicated, and so far only roughly approximate results have been obtained. But as the approach in most cases is statistical, usually based on a more or less simplified Thomas-Fermi model for the electrons of the moving ion, these approximations may be expected to fit better the measurements on ions having a high number of electrons--as in fission fragments, or even still more in the experiments described here, than the measurements for low- Z_1 ions. It has been predicted by Bohr⁶ that when very heavy particles penetrate a medium, the nucleus of a moving particle will carry throughout almost its whole path a large number of electrons, which (owing to continual capture and loss) fluctuates around an average value determined by the velocity and nuclear charge of the ion and by the properties of the medium. This has been verified experimentally for fission products. These fluctuations were expected to be a normal distribution. Our experimental data show that they may be approximated by a normal distribution as

$$\phi_z \approx \frac{1}{\sigma\sqrt{2\pi}} \exp \left[-(z-\langle z \rangle)^2 / 2\sigma^2 \right], \quad (7)$$

and this function is characterized by two parameters, the mean charge

$$\langle z \rangle = \sum_z \phi_z \times z, \quad (8)$$

and the distribution width

$$\sigma = \left[\sum_z \phi_z (z - \langle z \rangle)^2 \right]^{1/2} \quad (9)$$

which is related to the full widths at half maximum (w) of the distribution by

$$w = 2.354 \sigma.$$

The mean charge values $\langle z \rangle$ given in Table I were estimated according to Eq. (8). The differences obtained between $\langle z \rangle$ and z_{mp} for the same particle velocity are within the experimental accuracy, and all the distributions obtained may therefore be considered as practically symmetrical.

Figure 5 is a plot of the mean charge $\langle z \rangle$ as a function of particle mean velocity $\langle v \rangle$. It can be seen that in the velocity region studied the experimental points fit well, within the experimental error, a linear change of $\langle z \rangle$ with $\langle v \rangle$. No influence of $\Delta Z_1 = \pm 1$ could be found, within the experimental limits. The point for the lowest velocity measured ($\langle v \rangle = 2.52 \times 10^8$ cm/sec), which is for $Z_1 = 65$ (Tb), fits well the extrapolated line obtained for higher velocity values of $Z_1 = 66$ (Dy). The same applies for $Z_1 = 67$ (Ho), where resultant $\langle z \rangle$ values for two different velocities are shown. A more detailed comparison can be made for the results obtained for $\langle v \rangle = 4.24 \times 10^8$ cm/sec. For this velocity the charge-state distributions of Ho¹⁴⁹ particles and of Dy¹⁴⁹ particles, generated by two different nuclear reactions, have been studied in detail. It can be seen from Table II that the charge-state probabilities obtained for these two cases are practically identical. The estimate of the difference in binding energy of the electrons involved, calculated for the whole charge distribution, is about 3%, which is less than the experimental error. Therefore no significant influence on the results because of differences in $\Delta Z_1 = \pm 1$ could even be expected.

Considering the distribution width values (w) given in Table I shows that these values increase with increasing $\langle z \rangle$ values, but the ratio $w/\langle z \rangle$ remains almost constant within the experimental error, for the whole velocity region studied.

Let us now consider the dependence of $\langle z \rangle$ on v obtained on the basis of Bohr's theory on the stopping of fission fragments.^{6,9} This theory is based on a rough assumption that an ion of large Z_1 , when passing through matter, is stripped of all its orbital electrons that have velocities smaller than the translational velocity of the ion. Bohr uses, for the description of the ion constitution, a simplified statistical model of the Thomas-Fermi atom, obtaining an approximate expression for the velocity distribution of the larger part of the electrons bound in the ground state of a heavy ion of effective charge $\langle z \rangle$, corresponding to a considerable fraction of the nuclear charge. A rough estimate of the ionic mean charge is thus obtained from

$$\langle z \rangle = Z_1^{1/3} v/v_0, \quad (10)$$

applying to particle velocities in the region $v_0 < v < Z_1^{2/3}v_0$, where v_0 represents the velocity of the electron in the ground state of the hydrogen atom ($v_0 = \frac{e^2}{\hbar}$) and $Z_1^{1/3}$ stands for the "effective quantum number" ν of the binding state. However, it is essential for the applicability of $\nu = Z_1^{1/3}$ that $\langle z \rangle$ be somewhat smaller than $Z_1/2$. To apply Bohr's theory to our data, the "state of condensation" effect has to be taken into account. This effect depends, according to Bohr and Lindhard,¹⁰ upon the relative values of the time necessary for more uniform distribution of the energy of a few highly excited electrons, τ_{dis} and the time elapsing between two collisions, τ_{col} . For solids and liquids $\tau_{col} < \tau_{dis}$. According to Neufeld and Snyder¹⁷ an additional effect, the "distant collisions" effect, which causes autoionization, accounts partly for the "state of condensation effect." As the distribution of electronic orbital velocities in an ion that is continually perturbed by collisions at high frequency is not

known, Bohr and Lindhard,¹⁰ on the basis of qualitative considerations and Lassen's experimental results,¹² introduced into Eq. (10), for fission fragments, a semi-empirical factor of $3/2$.

When trying to compare the estimates obtained from Eq. (10) with experimental data for "very heavy" ions, we find that these are almost nonexistent. The few existing ones are summarized in Table III. As predicted,¹⁰ Eq. (10) does not fit the experimental data for Br ($Z_1=35$) and light fission fragments, but fits well for heavy fission fragments, where the use of $v = Z_1^{1/3}$ seems to be justified.

We have not performed any charge distribution measurements in low-pressure gas strippers for particles of $Z_1 = 66$. We assume that for the highest degree of ionization measured the conditions for the applicability of $v = Z_1^{1/3}$ are still fulfilled. Equation (10) will thus provide us an estimate for $\langle z \rangle$ in low-pressure gases. This would result in an increased empirical factor of the order of 2. This larger factor may be attributed to the higher Z_1 of the particles than of heavy fission fragments. This fits the experimental observation that the excess of ionization, as a result of the "state of condensations" effect for a certain velocity, increases with the nuclear charge of the ion.¹⁸

A theoretical estimate of $\langle z \rangle$ given by Brunning, Knipp, and Teller⁸ is based on a more detailed Thomas-Fermi statistical model. They assumed the characteristic velocity of the electron v_e to be roughly proportional to the particle velocity, and introduced an empirical factor of proportionality, γ . The characteristic velocity of the electron was calculated for two different assumptions: (a) the energetically most easily removable electron, (b) the outermost electron. In Fig. 6 the corresponding curves calculated for an ion of $Z_1 = 66$ are shown [curves (a) and (b)]. Curve (c) is according to Eq. (10) and curve (c) shows our experimental results, assuming $\gamma = 1$; the following γ values were obtained: For assumption (a) $\gamma = 4.9$ for $\langle v \rangle = 2.52 \times 10^8$ cm/sec, decreasing to $\gamma = 3.5$ for $\langle v \rangle = 5.97 \times 10^8$ cm/sec. Applying assumption (b), we see that for the whole velocity range measured, γ is close to unity, being

$$\begin{aligned} \gamma &= 1.2 & \text{for } \langle v \rangle &= 2.52 \times 10^8 \text{ cm/sec} & \text{and} \\ \gamma &= 0.92 & \text{for } \langle v \rangle &= 5.97 \times 10^8 \text{ cm/sec.} \end{aligned}$$

Even our results fit fairly well the curve based on assumption (b), it has to be remembered that Brunnings et al. approach is for an ion in the ground state and therefore can not directly apply to measurements in solids. The γ values obtained have to be considered as empirical ones, containing the ratio between what is assumed to be the characteristic velocity of the electron and the velocity of the ion, as well as the effect of the state of condensation. It can also be seen from Fig. 6 that the factor of about 2 obtained when applying Eq. (10) holds for the whole velocity region studied.

Electron capture and loss cross sections cannot be determined without a measurement for a nonequilibrium state. However, it is possible to determine the ratio of loss to capture cross sections for a particular electron from the equilibrium relation when the possibility of multiple electron transfer in a single collision is neglected:¹⁹

$$\frac{\phi_{z+1}}{\phi_z} = \frac{\sigma_{z,z+1}}{\sigma_{z+1,z}} = \frac{\sigma_{\text{loss}}}{\sigma_{\text{cap}}} \quad (11)$$

As an example, these ratios for $z = 6, 12, \text{ and } 18$ as a function of $\langle v \rangle$ are shown in Fig. 7. Within the experimental error limits these ratios fit the relation

$$\frac{\phi_{z+1}}{\phi_z} \propto v^{k_z}, \quad (12)$$

where k_z increases very slightly with z .

Bohr estimated that for heavy fission fragments penetrating heavy materials, these ratios are expected to be of the order of unity.⁹ Our results confirm this estimate.

Figure 8 shows a compilation of existing experimental data of the mean charge (z) of "very heavy" ions in solids as a function of particle velocity $v^{1/2}$. As well as representing our data for (z) by a linear relationship with v , we can also represent them fairly well as even a linear function of $v^{1/2}$.

Because of almost complete lack of experimental data for charge distributions of "very heavy particles," it is impossible at this stage to find even any empirical regularity for the mean charge of a particle as a function of its velocity and nuclear charge. Additional experimental data for particles of various Z_1 at various velocities are required before a phenomenological analysis of the results is possible and the existing approximate theories can be more closely examined.

In a forthcoming paper range-energy calculations of Dy^{149} particles, based on the data given here for effective charge distributions, will be presented and compared to existing range measurements.²

B. Nonequilibrium Charge Distributions

In the foregoing study of equilibrium charge distribution it was found that the necessary equilibrium target layer was of the order of $25 \mu\text{g}/\text{cm}^2$.

For the reaction $\text{Fr}^{141} (O^{16} \text{on}) \text{Ho}^{149}$ a number of experiments using thinner targets was performed.

In Fig. 9 some preliminary results are shown. As thinner targets are used a clear tendency of the mean charge toward a higher-than-equilibrium value can be seen. If the "instantaneous" charge of the compound nucleus were assumed equal to the charge of the fully stripped bombarding ion, an explanation for the additional ionization effect would have to be given. As internal conversion and orbital electron capture presumably will not be of any quantitative importance in this case, this effect may be attributed to the drastic "shaking" of the electron cloud following the sudden change of the nuclear charge by $\Delta Z_1 = 8$ as a result of the nuclear reaction.

However, further and more detailed experimental studies are needed before any conclusive and more quantitative statement can be made.

REFERENCES

* This work was performed under the auspices of the U. S. Atomic Energy Commission.

† On leave from Department of Nuclear Science, Israel Institute of Technology, Haifa, Israel.

1. B. G. Harvey, *Ann. Rev. Nucl. Sci.* 10, 235 (1960).
2. L. Winsberg and J. M. Alexander, *Phys. Rev.* 121, 518 and 529 (1961).
3. John M. Alexander and D. H. Sisson, Recoil Range Evidence for the Compound-Nucleus Mechanism in Reactions Between Complex Nuclei, UCRL-10098, (April 1962).
4. Jacques B. T. Read, Inge-Maria Ladenbauer-Bellis, and Richard Wolfgang, *Phys. Rev.* 127, 1722 (1962).
5. I. R. Bates and G. W. Griffing, *Proc. Phys. Soc. (London)* A68, 90 (1955).
6. N. Bohr, *Phys. Rev.* 58, 654 (1940).
7. W. E. Lamb, *Phys. Rev.* 58, 696 (1940).
8. J. E. W. Brunnings, J. Knipp, and E. Teller, *Phys. Rev.* 60, 657 (1941).
9. N. Bohr, *Kgl. Danske Videnskab. Selskab Mat. Fys. Medd.* 18, No. 8 (1948).
10. N. Bohr and G. Lindhard, *Kgl. Danske Videnskab. Selskab. Mat. Fys. Medd.* 28, No. 7 (1959).
11. I. S. Dmitriev, *Soviet Physics JETP* 51, 475 (1957).
12. N. O. Lassen, *Kgl. Danske Videnskab. Selskab. Mat. Fys. Medd* 30, No. 8 (1955).
13. C. B. Fulmer and B. C. Cohen, *Phys. Rev.* 109, 94 (1958).
14. H. H. Heckman, E. L. Hubbard, and W. G. Simon, Electron Charge Distributions for Heavy Ions at High Velocities, UCRL-10265, (May 1962).
15. G. N. Simonoff and J. M. Alexander, Angular Momentum Effects on Neutron Emission by Dy and Tb Compound Nuclei, UCRL-10099-Rev., (Sept 1962).
16. As Nd¹⁴² targets an enriched isotope of 97.4% isotopic purity was used. As Ba¹³⁸ targets BaCl₂ of enriched isotopic purity of 98.0% was used. The other targets used were the natural metals. All the targets were vacuum evaporated onto thin Al or Ni backing.

17. J. Neufeld and W. S. Snyder, Phys. Rev. 107, 96 (1957).
18. V. S. Nikolaev, I. S. Dmitriev, L. N. Fateeva, and Ya. A. Teplova, Soviet Physics JETP 12, 627 (1961).
19. Capture of several electrons in a single encounter has been observed recently by Nikolaev.²⁰
20. V. S. Nikolaev, L. N. Fateeva, I. S. Dmitriev and Ya. A. Teplova, Soviet Physics JETP 14, 67 (1962).
21. E. Almqvist, C. Broude, M. A. Clark, Y. A. Kuehner, and A. E. Litherland, Can. J. Phys. 40, 954 (1962).

Table I. Summary of experimental conditions and some results in charge distribution studies (symbols as used in text).

Nuclear reaction	E (lab) (keV)	Degraded thickness (mg/cm ² Al)	σ (mb)	Target thickness ($\mu\text{g}/\text{cm}^2$)	Z ₁	Z ₂	(v) × 10 ⁻⁸ (cm/sec)	velocity spread caused by		v	z _{mp}	\bar{z}
								Neutron evaporation	target thickness			
Pr ¹⁴¹ (C ¹² , ⁴ n)To ¹⁴⁹	64.0	{ 1.7 backing 36.0 Be degr }	35	103	65	59	2.52	9.3	3.2	7±1	9±1	9.7±0.4
Nd ¹⁴² (C ¹² , ⁵ n)Dy ¹⁴⁹	95.2		22.8	440	115	66	60	3.05	11.1	2.9	9±1	11±1
Nd ¹⁴² (C ¹² , ⁵ n)Dy ¹⁴⁹	112.0	10.5	170	115	66	60	3.30	12.2	2.7	9±1	12±1	12.9±0.4
Pr ¹⁴¹ (N ¹⁴ , ⁶ n)Dy ¹⁴⁹	105.7	19.9	295	103	66	59	3.45	10.9	2.6	9±1	12±1	13.6±0.4
Ce ¹³⁸ (O ¹⁶ , ⁷ n)Dy ¹⁴⁹	133.1	14.7	270	73	66	58	4.08	10.0	1.5	10±1	15±1	15.2±0.5
Ce ¹³⁸ (O ¹⁶ , ⁷ n)Dy ¹⁴⁹	141.0	11.6	262	73	66	58	4.24	10.8	1.4	10±1	16±1	16.0±0.5
Pr ¹⁴¹ (O ¹⁶ , ⁸ n)Ho ¹⁴⁹	144.5	10.1	180	103	67	59	4.24	10.3	1.8	10±1	16±1	16.1±0.5
Pr ¹⁴¹ (O ¹⁶ , ⁸ n)Ho ¹⁴⁹	162.0	2.1	200	103	67	59	4.50	10.6	1.7	11±1	17±1	17.6±0.5
La ¹³⁹ (F ¹⁹ , ⁹ n)Dy ¹⁴⁹	166.2	11.4	150	127	66	57	4.64	10.0	2.2	11±1	18±1	18.1±0.4
Ba ¹³⁸ (Ne ²⁰ , ⁹ n)Dy ¹⁴⁹	181.6	8.1	135	124	66	56	5.27	10.0	1.9	11±1	21±1	20.8±0.8
Ba ¹³⁸ (Ne ²² , ¹¹ n)Dy ¹⁴⁹	215.0	4.3	90	124	66	56	5.97	9.9	1.7	13±1	22±1	23.3±0.9

Table II. The relative probabilities of the different charge states β_z (%) for various particle velocities (symbols as used in text).

z_1	65	66	66	66	66	66	67	67	66	66	66
z_2	59	60	60	59	58	58	59	59	57	56	56
$\langle v \rangle \times 10^{-8}$	2.52	3.05	3.30	3.45	4.08	4.24	4.24	4.50	4.64	5.27	5.97
β_3 (%)	1.9±0.6	1.1±0.2									
β_4	2.8±0.9	1.3±0.3	1.1±0.2								
β_5	4.4±1.1	2.3±0.3	1.8±0.3	1.5±0.3	1.0±0.2	1.1±0.2	1.0±0.2				
β_6	6.0±1.2	3.0±0.4	2.5±0.3	2.0±0.3	1.4±0.2	1.5±0.2	1.5±0.2				
β_7	7.9±1.2	4.0±0.4	3.5±0.4	2.7±0.3	1.9±0.2	1.9±0.3	2.0±0.3	1.1±0.2	1.0±0.2		
β_8	10.2±1.1	5.6±0.6	4.6±0.5	3.7±0.4	2.6±0.2	2.4±0.3	2.7±0.3	1.3±0.2	1.2±0.2		
β_9	13.1±1.3	7.7±0.6	5.7±0.6	5.0±0.5	3.4±0.3	2.9±0.3	3.2±0.3	1.8±0.3	1.7±0.2	1.0±0.3	
β_{10}	12.9±1.3	8.7±0.6	7.1±0.5	6.7±0.5	4.5±0.4	3.6±0.3	4.1±0.3	2.4±0.3	2.4±0.3	1.4±0.4	
β_{11}	11.8±1.1	9.1±0.6	8.9±0.6	8.9±0.5	5.7±0.4	4.5±0.3	5.1±0.4	3.1±0.3	2.9±0.3	1.9±0.5	1.2±0.2
β_{12}	9.5±1.1	8.2±0.6	10.0±0.7	9.9±0.5	7.0±0.5	5.9±0.4	6.4±0.4	3.8±0.3	3.7±0.3	2.3±0.5	1.6±0.2
β_{13}	7.2±1.0	7.4±0.6	8.9±0.6	9.8±0.5	8.0±0.5	7.2±0.5	8.0±0.5	4.6±0.3	4.6±0.3	2.8±0.6	2.2±0.3
β_{14}	5.2±0.7	6.6±0.5	7.9±0.5	8.3±0.5	8.5±0.5	7.9±0.5	8.3±0.5	5.4±0.6	5.5±0.4	3.2±0.6	2.7±0.4
β_{15}	3.7±0.7	5.9±0.6	7.0±0.6	7.2±0.5	9.0±0.5	8.2±0.5	8.6±0.5	6.6±0.5	6.4±0.4	3.7±0.6	3.3±0.4
β_{16}	2.0±0.4	5.1±0.5	5.8±0.6	6.1±0.5	8.1±0.5	7.4±0.5	7.8±0.5	7.5±0.5	7.1±0.4	4.2±0.5	3.9±0.5
β_{17}		4.5±0.5	5.1±0.6	5.1±0.5	7.4±0.5	7.2±0.5	7.2±0.5	8.2±0.5	7.5±0.4	4.9±0.5	4.5±0.5
β_{18}		3.9±0.4	4.1±0.5	4.3±0.4	6.7±0.6	6.5±0.5	6.2±0.5	8.1±0.5	7.9±0.4	5.6±0.5	5.2±0.6
β_{19}		3.2±0.5	3.6±0.4	3.6±0.4	6.0±0.6	5.9±0.4	5.5±0.4	7.8±0.5	7.7±0.4	6.4±0.6	5.8±0.6
β_{20}		2.6±0.4	2.9±0.4	3.0±0.4	5.1±0.5	5.2±0.4	5.0±0.4	7.1±0.5	7.2±0.4	7.1±0.6	6.5±0.7
β_{21}		2.1±0.3	2.4±0.3	2.6±0.3	4.0±0.4	4.3±0.3	4.0±0.3	6.2±0.5	6.5±0.4	7.6±0.6	7.1±0.6
β_{22}		1.7±0.3	2.0±0.3	2.1±0.3	3.2±0.6	3.3±0.3	3.1±0.3	5.5±0.4	5.7±0.4	7.4±0.6	7.4±0.6
β_{23}		1.3±0.3	1.5±0.2	1.7±0.2	2.3±0.3	2.7±0.3	2.4±0.3	4.5±0.3	4.8±0.3	6.9±0.6	7.2±0.7
β_{24}		1.0±0.2	1.0±0.2	1.3±0.2	1.6±0.3	2.1±0.3	2.0±0.3	3.7±0.3	3.9±0.3	6.2±0.6	6.8±0.7
β_{25}				1.0±0.2	1.2±0.2	1.7±0.2	1.6±0.2	3.1±0.3	3.0±0.3	5.2±0.5	6.1±0.6
β_{26}						1.3±0.2	1.2±0.2	2.4±0.3	2.3±0.3	4.3±0.5	5.5±0.6
β_{27}						1.0±0.2	1.0±0.2	1.8±0.3	1.7±0.2	3.7±0.6	4.7±0.6
β_{28}								1.2±0.2	1.3±0.2	3.2±0.6	3.9±0.5
β_{29}									1.0±0.2	2.7±0.6	3.3±0.4
β_{30}										2.3±0.5	2.9±0.4
β_{31}										1.9±0.5	2.5±0.3
β_{32}										1.5±0.4	1.9±0.3
β_{33}										1.1±0.3	1.5±0.2

Table III. Some experimental and theoretical \bar{z} values for "very heavy" ions.

Z_1	$v \times 10^{-8}$ (cm/sec)	\bar{z} (in positive electron units)			
		gas		solid	
		Experimental	Theoretical ^a	Experimental	Theoretical ^b
35 (Br) ^c	6.00	--	8.9	11.0	13.3
38 (Light fission fragments) ^d	11.00	13.8	16.8	19.2	25.2
54 (heavy fission fragments) ^d	6.60	10.5	11.3	17.8	17.0
	8.80	14.6	15.1	22.5	22.6
66 (Dy)	5.97	--	11.0	23.3	16.5

^aAccording to Eq. (10) by Bohr.

^bEquation (10) and factor $3/2$ by Bohr and Lindhard.

^cReference 21.

^dReferences 12, 13.

FIGURE CAPTIONS

Fig. 1. Schematic diagram of experimental arrangement.

Fig. 2. Experimental scanning curve - horizontal displacement of particles on catcher foil - x , as a function of α particle track density. Nuclear Reactions: $\text{Pr}^{141}(O^{16}\text{Sn})\text{Ho}^{149}$ $E_p(\text{lab}) = 162.0 \text{ MeV}$; Target thickness = $100 \mu\text{g}/\text{cm}^2$. Mean velocity of Ho^{149} particles: $\langle v \rangle = 4.5 \times 10^8 \text{ cm/sec}$. Magnetic field strength = 3150 gauss.

Fig. 3. Corrected charge distribution histogram. Relative probability $\phi_z(\beta)$ as a function of the effective charge state z (in positive electron units). Nuclear charge of particles: $Z_1 = 67$; Mean velocity of particles: $\langle v \rangle = 4.5 \times 10^8 \text{ cm/sec}$.

Fig. 4. Relative probabilities for some of the charge states obtained - $\phi_z(\beta)$ as a function of the mean velocity of the particles $\langle v \rangle$.

$$z = 5, 10, 15, 20, 25$$

$$Z_1 = 66 \pm 1$$

$$Z_2 = 56 \longrightarrow 60$$

See Table I

Fig. 5. Mean charge $\langle z \rangle$ as a function of mean velocity of particles $\langle v \rangle$. Nuclear charges of moving particles: $Z_1 = 65, 66, 67$.

Fig. 6. Degree of ionization $\langle z \rangle / Z_1$ as a function of the velocity characteristic of the process of electron capture and loss.

Fig. 7. Ratio of adjacent charge state probabilities as a function of mean velocity of particles for $z = 6, 12$ and 18 .

Fig. 8. Compilation of existing experimental data of the mean charge $\langle z \rangle$ of "very heavy" ions as a function of particle velocity $v^{1/2}$.

Fig. 9. The mean charge $\langle z \rangle$ of Ho^{149} particles as a function of target thickness; Nuclear Reaction: $\text{Pr}^{141}(O^{16}\text{Sn})\text{Ho}^{149}$. Particle mean velocity: $\langle v \rangle = 4.5 \times 10^8 \text{ cm/sec}$.

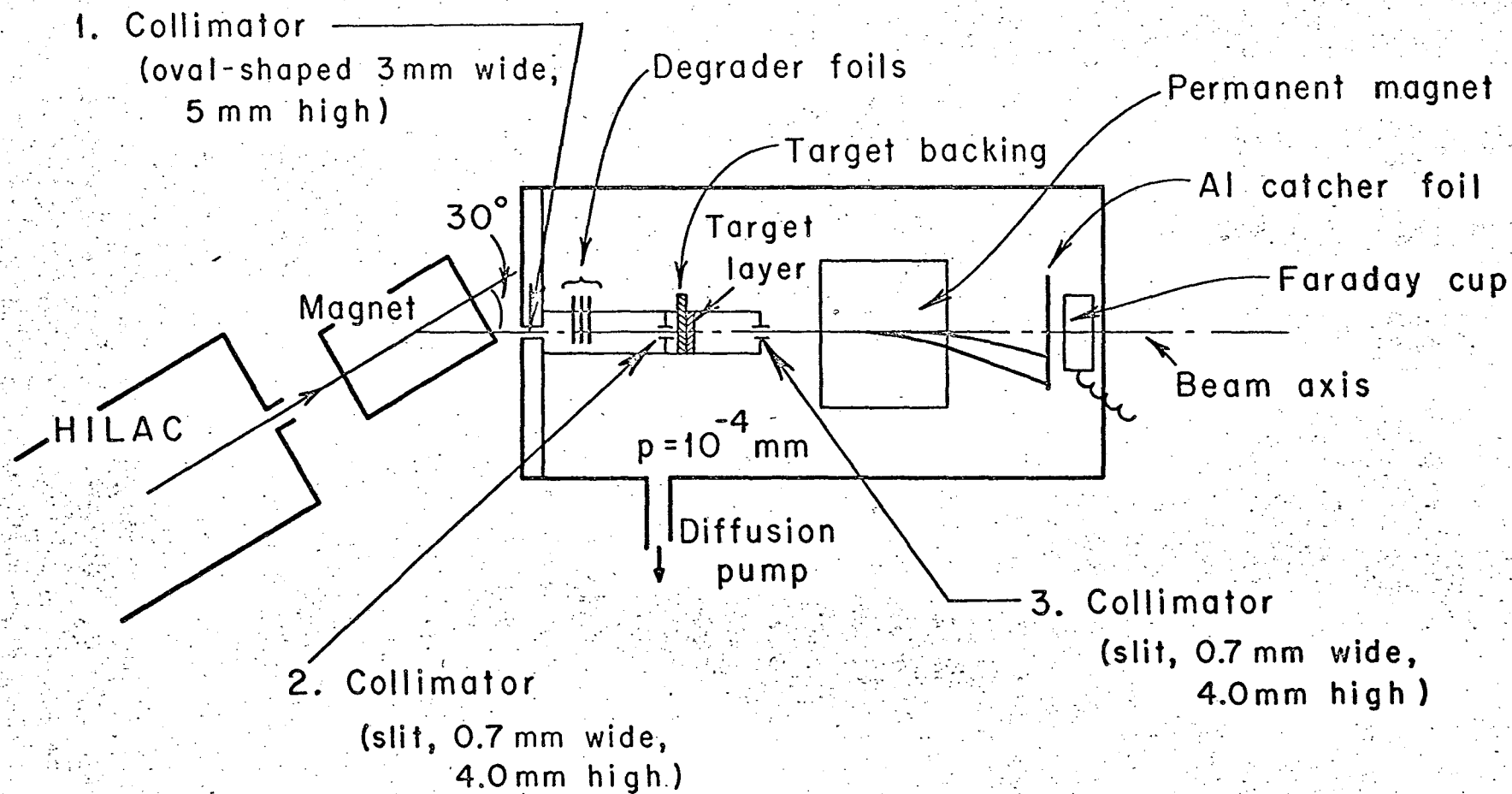


Fig 1

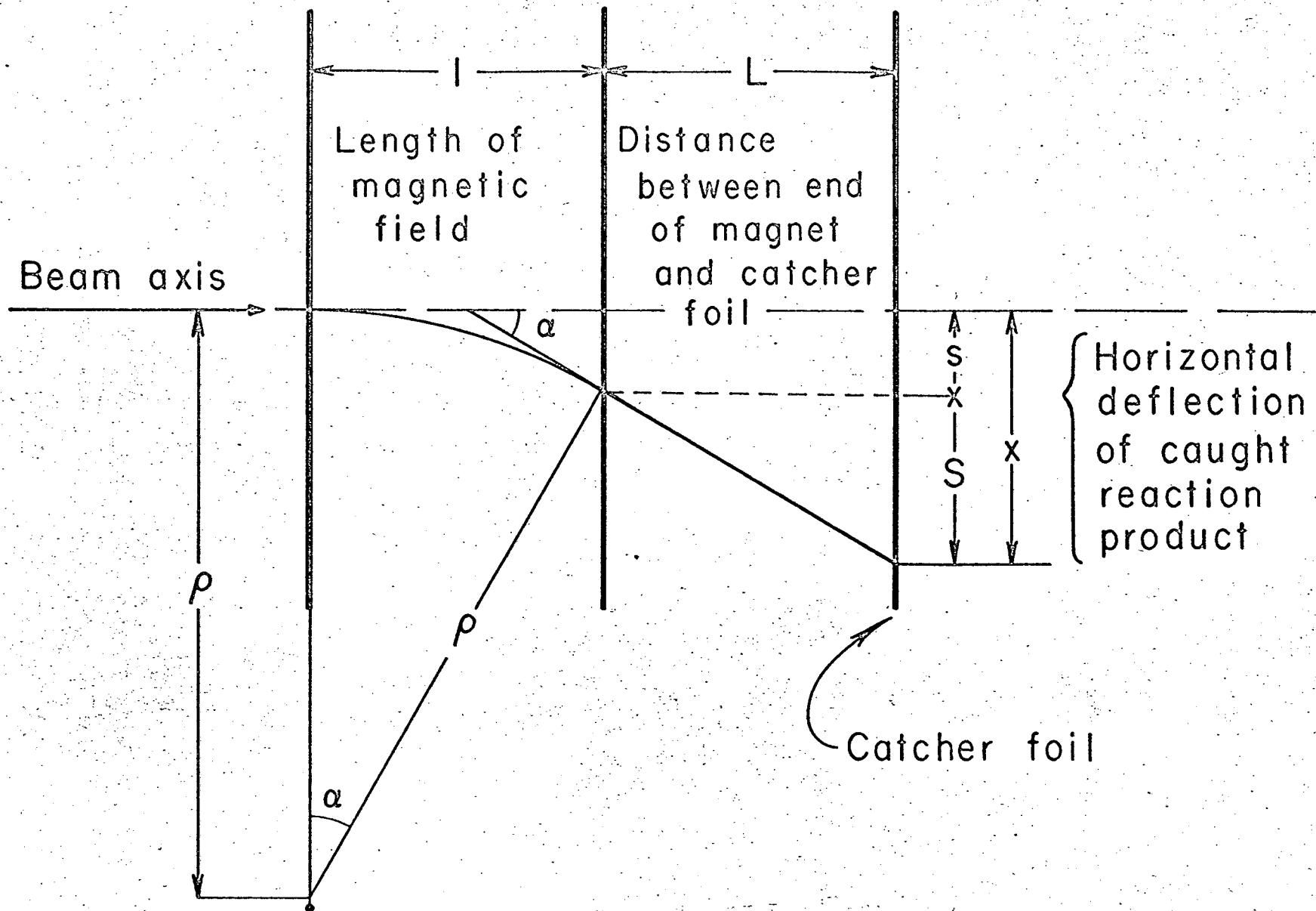
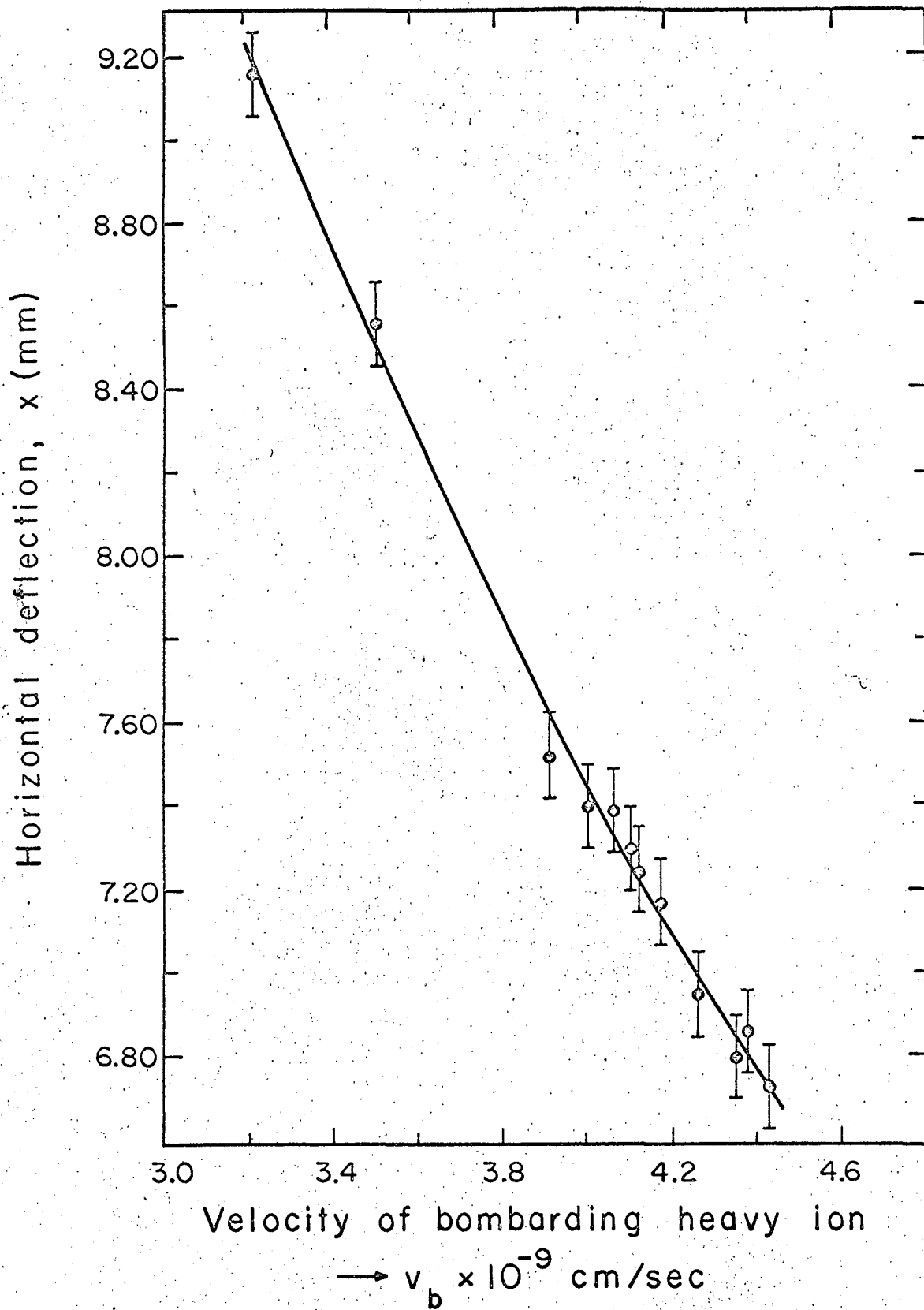
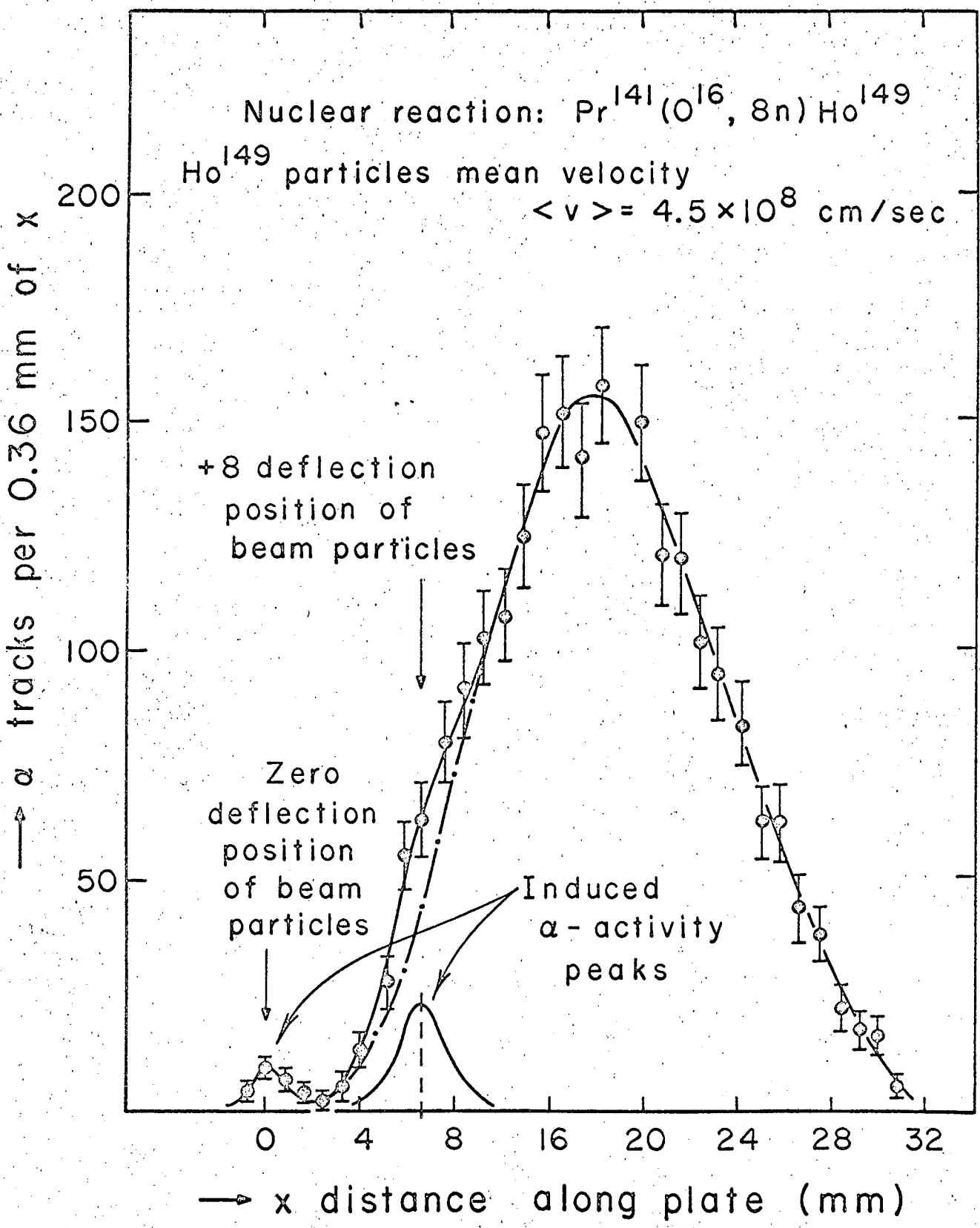


Fig 2



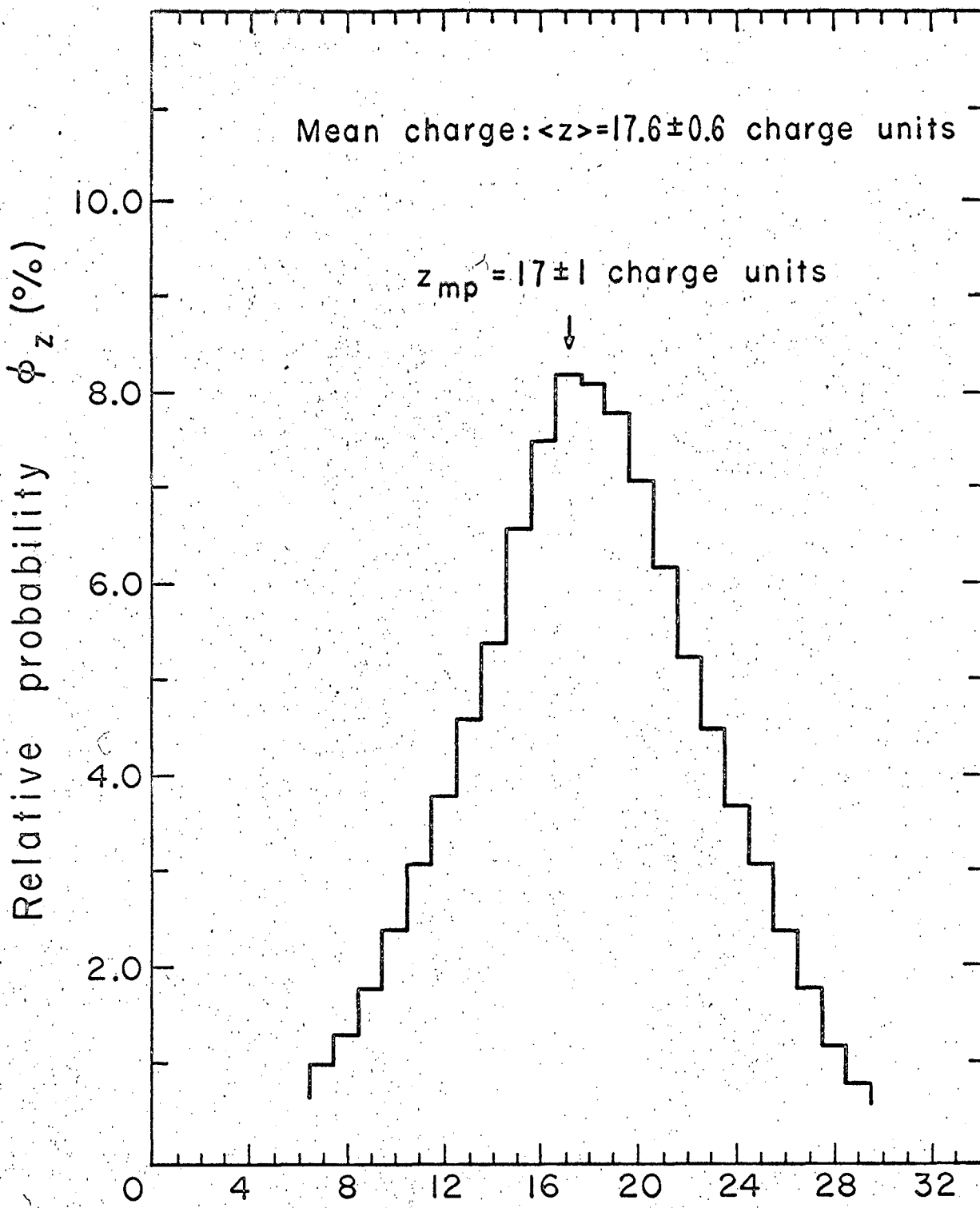
MU-29998

Fig 3



MU-29999

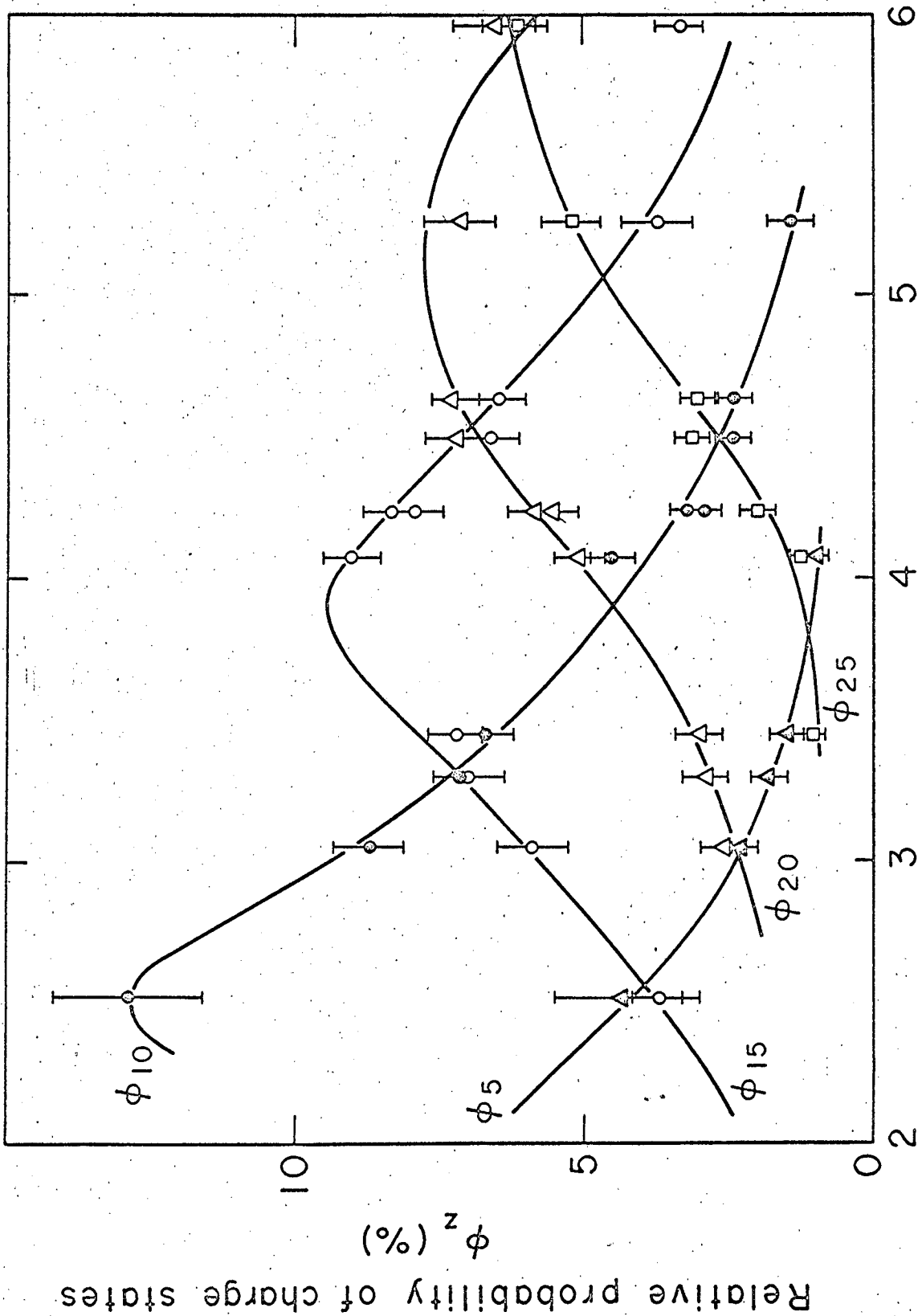
Fig 4



→ z effective charge state in positive electron units

MU-30000

Fig 5



Mean velocity of particles $\bar{v} \times 10^{-8}$ cm/sec

MU-30001

Fig 6

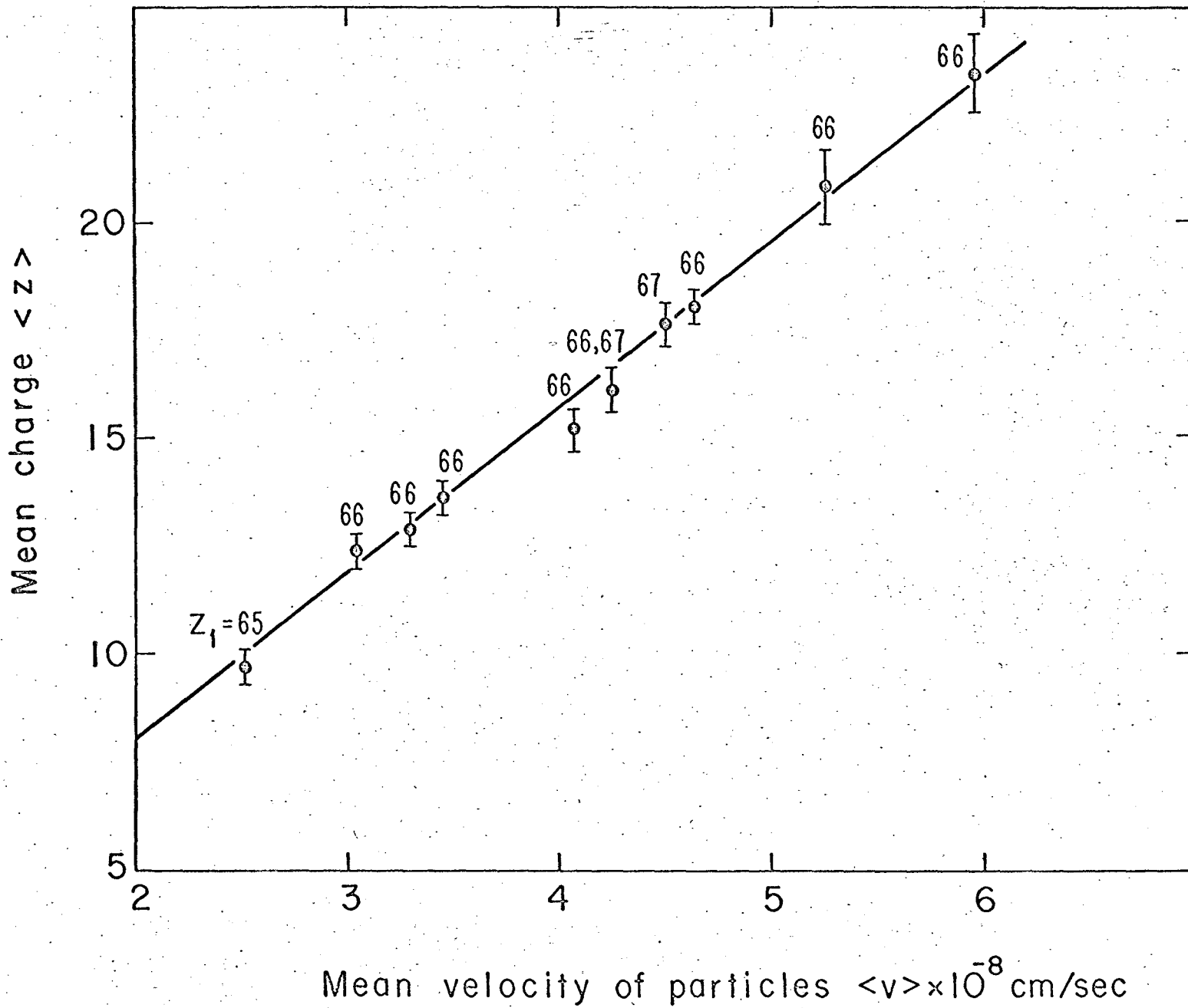


Fig 7

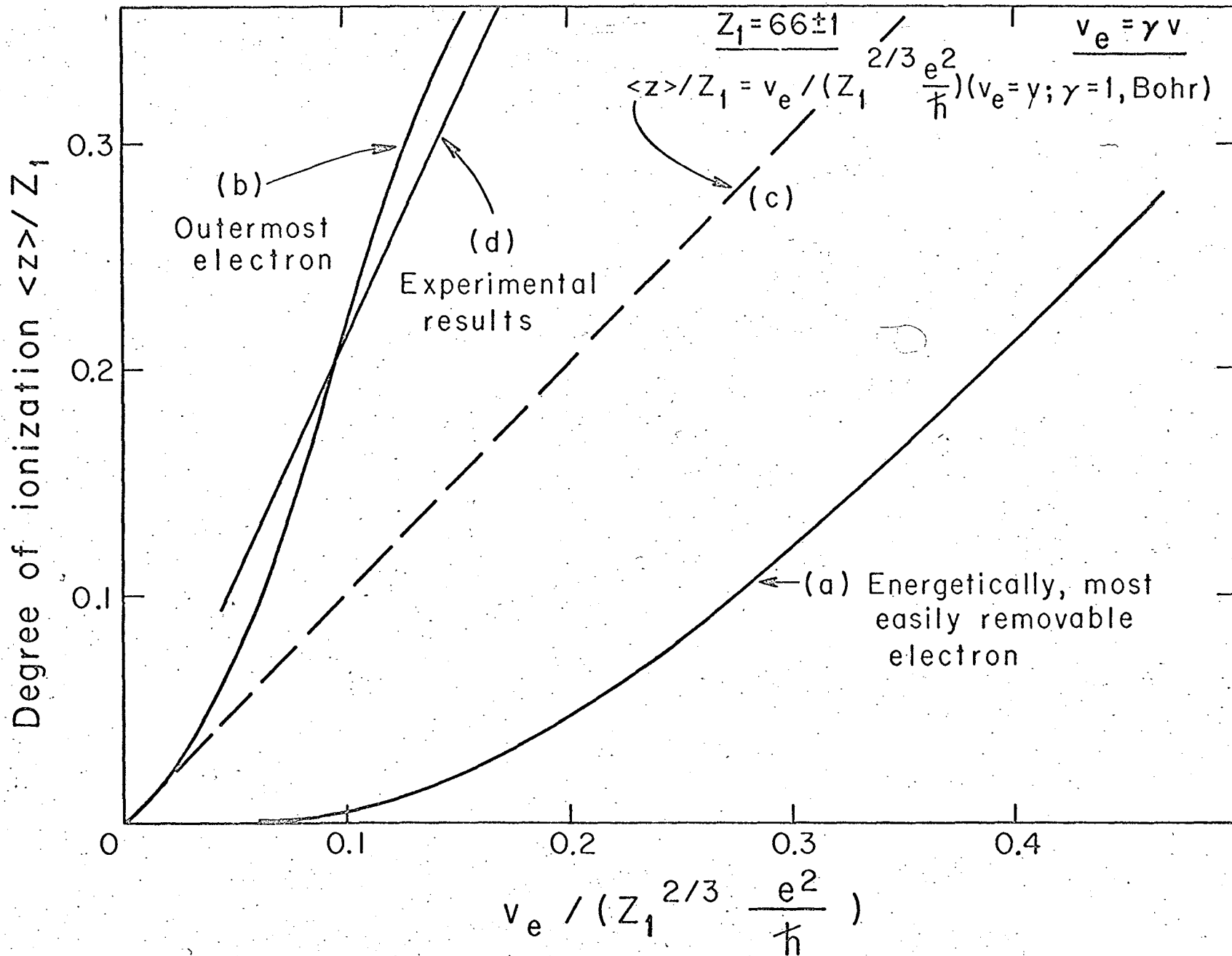


Fig 8

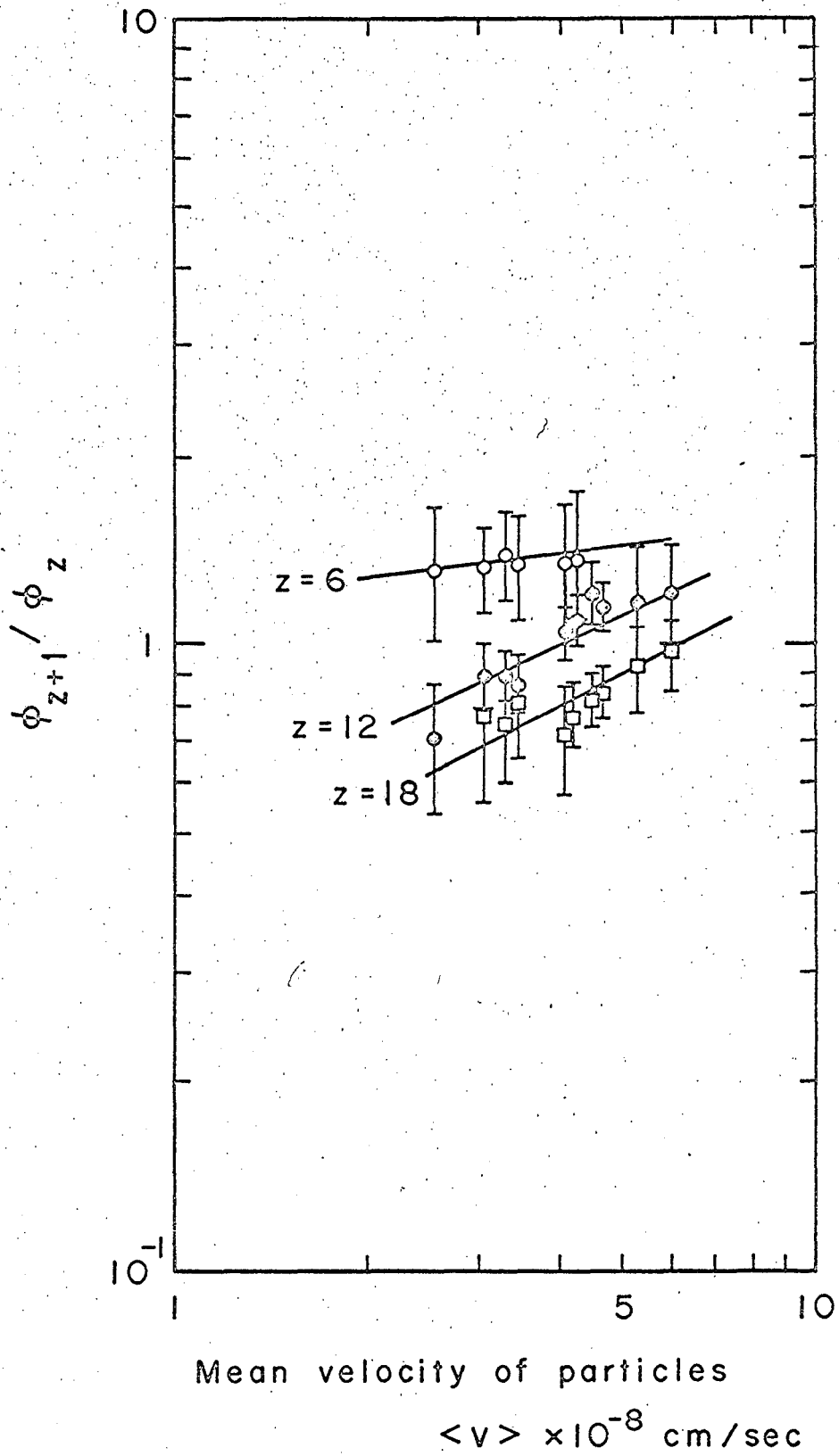
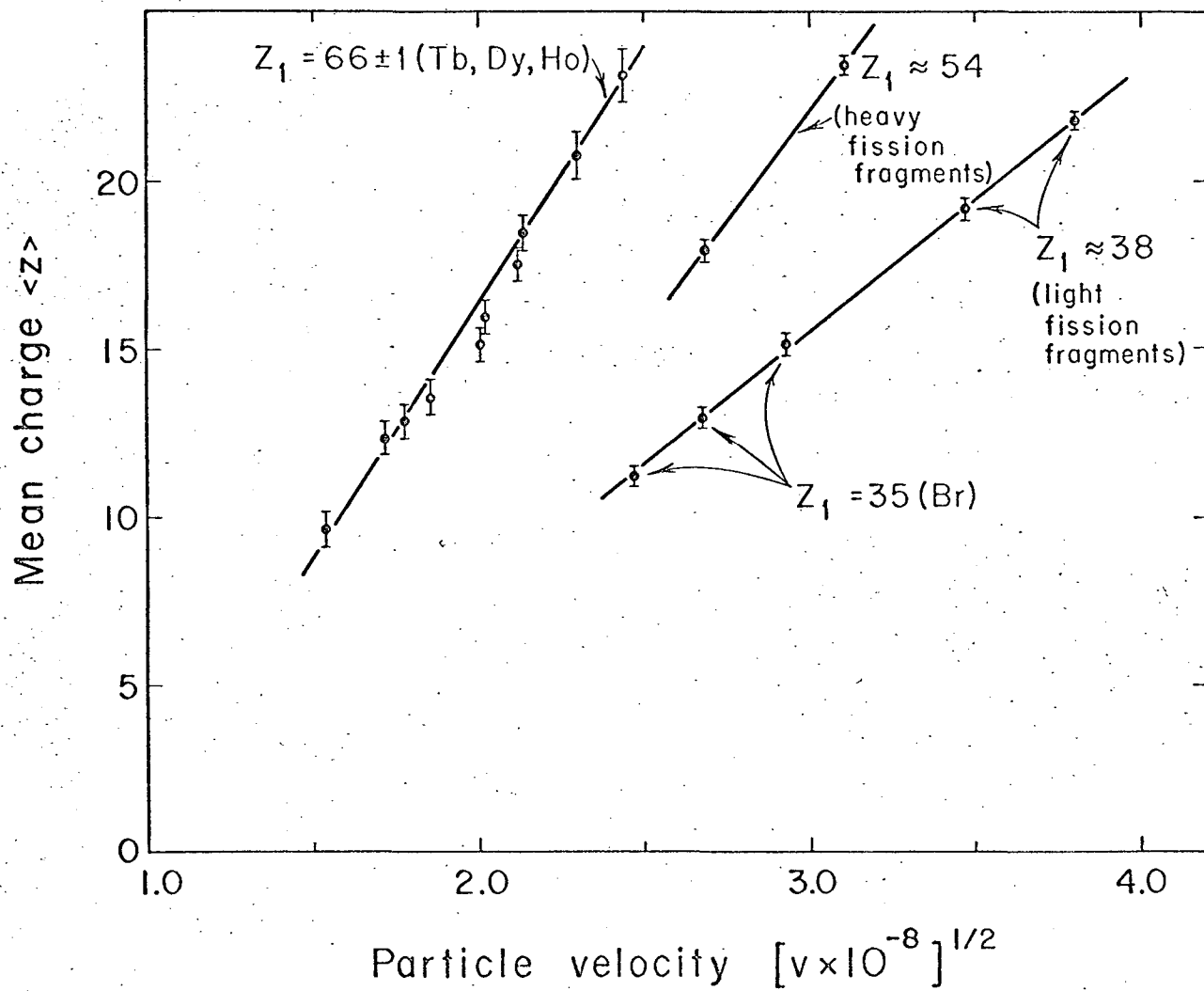


Fig 9



MUB-1688

Fig 10

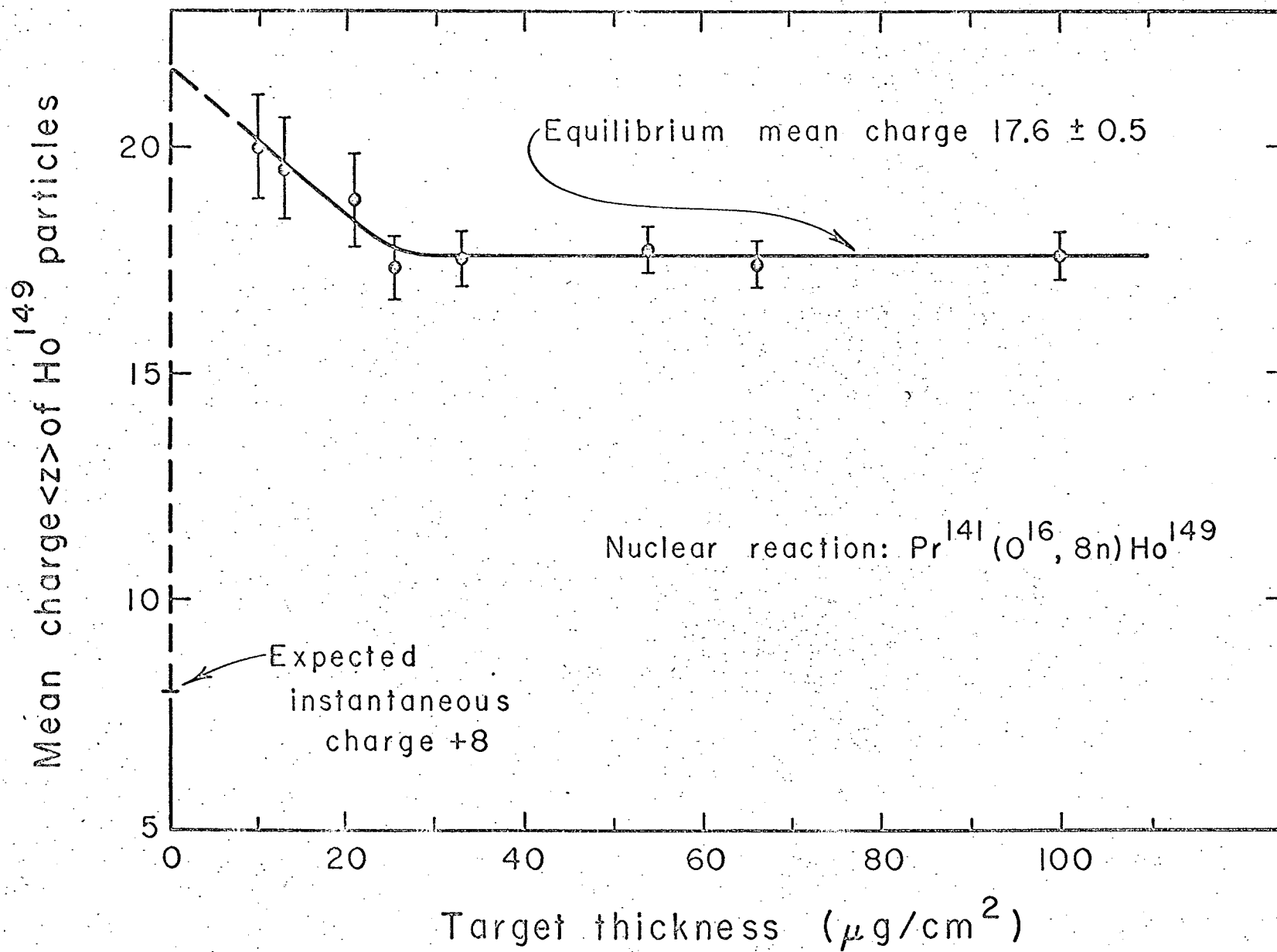


Fig 11



100

100